

# Actuation Requirements of Swashplateless Trailing-Edge Flap Helicopter Rotor in Maneuvering and Autorotation Flights

Jinwei Shen

*Staff Scientist*

National Institute of Aerospace

Hampton, VA

Inderjit Chopra

*Alfred Gessow Professor & Director*

Alfred Gessow Rotorcraft Center

Department of Aerospace Engineering

University of Maryland, College Park, MD

This paper examines the actuation requirements of trailing-edge flap system as primary flight control device for an ultralight helicopter rotor in maneuvering and autorotation flights. The swashplateless design is implemented by modifying a two-bladed teetering rotor of an ultralight helicopter through the use of plain flaps on the blades, and by replacing the pitch link. A comprehensive rotorcraft analysis based on UMARC is carried out to obtain the results for the swashplateless rotor configuration. Wind tunnel trim procedure is adopted to simulate maneuvering and autorotation flight conditions. It is concluded that the required trailing-edge flap deflections and actuation power are moderate in maneuvering and low speed autorotation flights, and the selection of optimum blade index angle need to be a comprise among steady-level and maneuvering flight conditions.

## Notation

$M_h$	Trailing-edge flap hinge moment
$M_t$	Main rotor shaft torque
$N_b$	Number of rotor blades
$P_f$	Trailing-edge flap actuation power
$\alpha_s$	Longitudinal rotor shaft tilt
$\beta_{T1c}$	Lateral cyclic rotor teetering angle
$\beta_{T1s}$	Longitudinal cyclic rotor teetering angle
$\delta$	Trailing-edge flap deflection
$\delta_0$	Trailing-edge flap collective angle
$\delta_{1c}$	Trailing-edge flap lateral cyclic
$\delta_{1s}$	Trailing-edge flap longitudinal cyclic
$\delta^*$	Trailing-edge flap rate
$\mu$	Advance ratio
$\psi$	Azimuth angle
$\sigma$	Rotor solidity
$\theta$	Blade pitch angle
$\theta_{index}$	Blade index angle
$\theta_{root}$	Blade pitch motion at root spring

## Introduction

The use of a trailing-edge flap rotor for primary flight control appears attractive in the context of an actively controlled rotor. The embedded flaps can perform multiple functions, such as vibration reduction (Refs. 1–6), automated in-flight tracking (Ref. 7), and primary flight control (Ref. 8). A trailing-edge flap system was the primary candidate in the NASA Revolutionary Concepts (RevCon) program of “swashplateless helicopter flight”. The conventional helicopter mechanical control system typically consists of rotor swashplate, pitch links and pushrods, and fixed system hydraulic flight control actuators. This system contributes significantly to the weight, drag, and maintenance cost of the aircraft, and hence degrades the overall mission performance, reduces service life, and increases operating cost. Experiments conducted by Barrett *et al.* (Ref. 9) on a model helicopter achieved a 26% reduction in parasitic drag, 40% reduction in flight control system weight, and 8% reduction in total aircraft gross weight by eliminating the swashplate assembly.

A recent study by Ormiston, using a simple rigid rotor model, explored the feasibility of a swashplateless rotor with plain trailing-edge flaps (Ref. 10). This study identified that the blade fundamental torsional frequency need to be lowered to values in the neighborhood of 1.5

---

Presented at the American Helicopter Society 60th Annual Forum, Baltimore, Maryland, June 7-10, 2004. Copyright © 2004 by the American Helicopter Society International, Inc. All rights reserved.

to 2.5/rev, and pitch index angle (pre-collective) need to be incorporated for the implementation of this concept. In a recent study, the authors developed a comprehensive analysis (Refs. 11, 8) for a swashplateless rotor with trailing-edge flaps based on UMARC (University of Maryland Advanced Rotorcraft Code). The analysis was carried out on a five-bladed bearingless rotor system (MD 900) with a soft pitch link (control frequency of 2.1/rev) for the wind tunnel trim conditions. The plain flaps were shown to have the capability of performing both primary rotor control, and active vibration control functions. Blade pitch index angle, blade root spring stiffness, trailing-edge flap location and size (length and chord ratio) were found to be key parameters in the design of a swashplateless rotor with trailing-edge flaps. Overall, the swashplateless rotor was found to be more aeroelastically stable than the conventional rotor. For the swashplateless concept investigation of RevCon program, the authors present the studies of utilizing trailing-edge flap for primary control of an ultralight helicopter (ASI 496) (Refs. 12, 13). The simulations were carried out for the two-bladed teetering rotor with trailing-edge flaps with free flight trim conditions. Through parametric studies, key design variables, such as blade index angle, flap location and geometry (size and length), were optimally selected for the swashplateless concept. The rotor performance was compared between the swashplateless rotor design and the baseline rotor with conventional swashplate control. Most of present analyses of swashplateless rotor system were carried out in steady level flight conditions. The required trailing-edge flap angles and actuation power in maneuvering and autorotation flight conditions may be quite severe as compared to those for steady level flight condition. A parametric study in these flight conditions is necessary for the design and development of a swashplateless system.

The objective of the present study is to investigate systematically the control effectiveness and actuation requirement of trailing-edge flap system for primary control in maneuvering and autorotation flights, and identify key design variables that may impact the development of a swashplateless rotor system.

## Analytical Model

The baseline rotor configuration for the swashplateless configuration is the ASI 496 (Table 1), an ultralight sport helicopter. It utilizes a two blade teetering rotor design and has a normal gross weight of 912 lbs and a cruise speed of 61 knots ( $\mu = 0.16$ ). The existing conventional swashplate controlled system consists of blades with a rotating blade torsional frequency of 2.2/rev. The proposed swashplateless rotor design modifies the

Table 1: ASI 496 rotor properties

Property	Value
Rotor Type	Teetering
Number of Blades	2
Rotor Diameter	23 ft.
Rotor Speed	525 RPM
Chord	6.7 inch
Linear Twist Angle	$-8^\circ$
Lock Number	5.01
Solidity	0.0309
Undersling	3.45 inch
Weight	912 lb
Cruise Speed	61 knots
Blade index angle	$18^\circ$

baseline rotor by replacing the swashplate assembly with a root spring that torsionally restrains the blade root near the hub. The root spring stiffness is carefully selected to give the same blade torsional frequency as the baseline conventional rotor so that blade dynamic characteristics are kept unaltered.

The baseline rotor analysis is adapted from UMARC. The modeling of the swashplateless teetering rotor with trailing-edge flaps in free flight steady trim is discussed in Refs. 12 and 13. The present study incorporates wind tunnel trim procedure to simulate maneuvering and autorotation flight conditions (Ref. 14). The following briefly outlines the analysis and solution procedure adopted. The analysis incorporates finite element methodology in space and time. In the analysis of the teetering rotor, it is necessary to treat both blades simultaneously because the blades are rigidly connected to each other and attached to the mast through a common flapping hinge (Ref. 15). The blade is modeled as an elastic beam undergoing flap bending, lag bending, elastic twist, and axial deformation. The rotor blades are discretized into a finite number of beam elements, each with 15 degrees of freedom. Nineteen aerodynamic/structural elements are used to model the main blade. Eight time elements with fifth order shape functions are used to calculate the coupled trim solution. Trailing-edge flap aerodynamic and inertial effects are included both in the formulation of the blade equations of motion and the hub loads computation.

For a rotor with flaps for primary controls, the control angle input to a flap is given by;

$$\delta(\psi) = \delta_0 + \delta_{1c} \cos \psi + \delta_{1s} \sin \psi \quad (1)$$

and the blade pitch angle consists of the blade index angle plus the pitch induced by flap control inputs (Fig. 1);

$$\theta(\psi) = \theta_{index} + \theta_{root}(\psi) \quad (2)$$

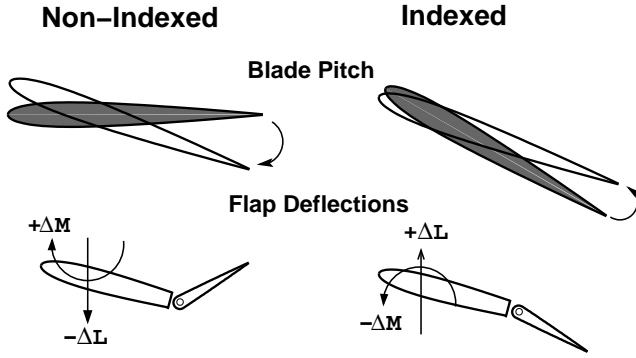


Figure 1: Blade pitch indexing

The flap control angles are obtained from the coupled trim procedure. The coupled analysis determines the blade response given a set of controls, shaft orientation, and inflow, and provides the blade loads together with the fixed system hub loads. In turn, these loads and responses are used in a separate set of equations representing either the vehicle free-flight equilibrium, or a prescribed wind tunnel operating condition. These equations govern the rotor control settings.

The present analysis incorporates wind tunnel trim procedure to simulate maneuvering and autorotation flight conditions. The maneuvering flight conditions are simulated with different rotor thrust level as indication of g-level. The rotor shaft tilt angles are chosen to resemble different maneuvering flight conditions such as ascending and descending flights. Autorotation flights are simulated with wind tunnel trim with that the selected shaft title angles generate zero rotor mast torque.

The wind tunnel trim adopted involves adjusting the controls to achieve zero 1/rev blade teetering angle, and a prescribed  $C_T/\sigma$  value with prescribed shaft angles. This can be expressed as a system of equations:

$$\mathbf{F}(\boldsymbol{\theta}) = \boldsymbol{\beta} - \boldsymbol{\beta}_{prescribed} = \mathbf{0} \quad (3)$$

where  $\boldsymbol{\theta} = \{\delta_0 \ \delta_{1c} \ \delta_{1s}\}$ ,  $\boldsymbol{\beta} = \{C_T/\sigma \ \beta_{T1c} \ \beta_{T1s}\}$ . The value of  $\boldsymbol{\theta}$  that satisfies equation (3) is determined iteratively using the Newton-Raphson method:

$$\boldsymbol{\theta}_{i+1} = \boldsymbol{\theta}_i + \Delta\boldsymbol{\theta}_i \quad (4)$$

where  $\Delta\boldsymbol{\theta}_i$  is obtained with equation (3) linearized about the trim controls using a Taylor's series expansion:

$$\mathbf{F}(\boldsymbol{\theta}_i + \Delta\boldsymbol{\theta}_i) = \mathbf{F}(\boldsymbol{\theta}_i) + \frac{\partial \mathbf{F}}{\partial \boldsymbol{\theta}} \Big|_{\boldsymbol{\theta}=\boldsymbol{\theta}_i} \Delta\boldsymbol{\theta}_i \quad (5)$$

The Jacobian matrix  $\frac{\partial \mathbf{F}}{\partial \boldsymbol{\theta}}$  used in equation (5) is obtained via a forward difference method by perturbing the individual controls in  $\boldsymbol{\theta}$ . The initial value for the trim algorithm is provided by a reduced order rigid blade response model that includes trailing-edge flap. The

Table 2: ASI 496 rotor trailing-edge flap properties

Property	Value
Flap Type	Plain Flap
Spanwise Length	25 inch (0.18R)
Chordwise Size	25 % (Blade Chord)
Flap Midspan Location	0.82R

trim solution and blade responses are updated iteratively until the convergence criteria are reached. To avoid numerical divergence during the iterations, the control angles are only updated when the blade responses converge under a certain throttle setting. The aerodynamic model of an airfoil with a plain trailing-edge flap used in present analysis was developed by Hariharan and Leishman (Ref. 16). This model, based on the Theodorsen model (Ref. 17), uses an indicial method and includes compressibility and unsteady effects. The Hariharan-Leishman model can predict sectional lift, drag, pitching moment, and hinge moment coefficient as a function of flap chord ratio, angle of attack, flap angle, and unsteady airfoil and flap motion. The Drees linear inflow is used to obtain the induced inflow distribution over the rotor disk. The incremental lift and pitching moment of an active trailing-edge flap, consisting of both inertial and aerodynamic contributions, are included in this coupled trim procedure.

Autorotation flights are simulated with wind tunnel trim by adjusting shaft tilt angle to achieve zero rotor mast torque. Eq. 3 is modified to include longitudinal shaft tilt angle, where  $\boldsymbol{\theta} = \{\delta_0 \ \delta_{1c} \ \delta_{1s} \ \alpha_s\}$ ,  $\boldsymbol{\beta} = \{C_T/\sigma \ \beta_{T1c} \ \beta_{T1s} \ M_t\}$ .

The actuation power of the flap system is calculated by integrating the product of the hinge moment and flap deflection rate over one complete rotor revolution:

$$P_f = \frac{N_b}{2\pi} \int_0^{2\pi} \max(-M_h \dot{\delta}, 0) d\psi \quad (6)$$

The actuation power presented in Eq. 6 is “ideal” because it only includes the energy used to drive the flap system, and neglects the heat dissipation of the smart actuators.

## Results and Discussion

The selected normal weight are 912 lbs which gives a  $C_T/\sigma$  of 0.075. The baseline trailing-edge flap characteristics are given in Table 2, and the flap has no aerodynamic balance (Ref. 18) in this study ( $c_b = 0$  in Fig. 2). Trailing-edge flap motion is positive for downward deflection, and hinge moment is positive when its direction is “nose-up” (and “tail-down”).

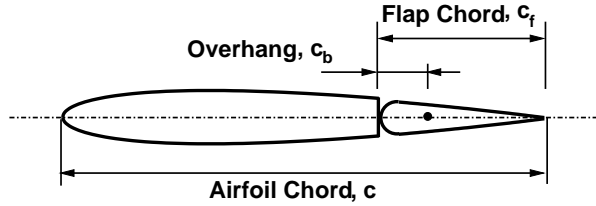


Figure 2: Trailing-edge flap

## Comparison of wind tunnel trim and propulsive trim

Figure 3 compares swashplateless rotor control settings for the complete range of advance ratios ( $\mu = 0$  to 0.17) between using wind tunnel trim and propulsive trim procedures. The wind tunnel trim procedure uses prescribed thrust level ( $C_T/\sigma$ ) and shaft angles to simulate forward flight conditions. The thrust level and longitudinal shaft tilt angles are listed in Table 3, and are predicted by the propulsive trim procedure. The lateral shaft tilt angles are set to zero in wind tunnel trim procedure. The swashplateless rotor has a pitch index angle of  $18^\circ$ , which yields small collective flap at the cruise speed 61 knots ( $\mu = 0.16$ ).

Figure 3(a) presents the collective trailing-edge flap deflection required to trim the swashplateless rotor using wind tunnel trim and propulsive trim procedures. The collective flap angle predicted by wind tunnel trim procedure shows the same trend as the propulsive trim. At low advance ratio ( $\mu \leq 0.08$ ), the collective flap angle of wind tunnel trim shows the same values as the propulsive trim. The difference between collective predictions of wind tunnel and propulsive trim increases with flight speed at high advance ratio ( $\mu \geq 0.1$ ). The difference may be attributed to the absence of lateral shaft tilt and tail rotor effects in the wind tunnel trim procedure. Figure 3(b) illustrates that the lateral cyclic trailing-edge flap deflections predicted by wind tunnel trim shows the same trend as the propulsive trim. At high advance ratios ( $\mu \geq 0.1$ ), the lateral cyclic flap angle of wind tunnel trim shows smaller value than that of the propulsive trim. Figure 3(c) shows the longitudinal cyclic flap angle required to trim the swashplateless rotor using wind tunnel trim and propulsive trim procedures. Similarly, the result of wind tunnel trim simulations compares well with the result of propulsive trim procedure at low advance ratios and shows increasing difference as advance ratio increases. The differences of cyclic flap angles between predictions of wind tunnel trim and propulsive trim is because the objective of cyclic flap angles are different between the two trim procedures. In wind tunnel trim, cyclic flap angles are used to cancel 1/rev rotor teetering

Table 3: Prescribed shaft angles and thrust levels in different forward speeds. (Positive is tilt forward)

Advance Ratio	Shaft Angle	Thrust Level
$\mu$	$\alpha_s$ (deg.)	$C_T/\sigma$
0	0.00	0.07506
0.027	0.24	0.07504
0.053	0.90	0.07506
0.080	2.00	0.07524
0.107	3.44	0.07534
0.133	5.04	0.07591
0.160	6.86	0.07693
0.173	7.76	0.07761

angles whereas in propulsive trim, they are used to control the direction of rotor thrust force to achieve steady level flight. However, Figure 3 shows the trailing-edge flap control angles of wind tunnel trim overall shows the same trend with the propulsive trim, and wind tunnel trim procedure may be used as a means of evaluating rotor and trailing-edge flap characteristics.

## Maneuvering Flights

Swashplateless rotor with trailing-edge flaps in maneuvering flights are simulated using wind tunnel trim by prescribed various g-levels (determined by rotor thrust levels) and rotor shaft angles. The effect of pitch index angles on actuation requirements of trailing-edge flap system is also investigated in maneuvering flight conditions.

Figure 4 shows the trailing-edge flap angles and actuation power required at different g-level maneuvering flights. The pitch index angle of 18 degrees is used in this simulation. Figure 4(a) presents the collective flap angles required for two flight speeds ( $\mu = 0.08$  and 0.16) in maneuvering flights. The collective flap angles are all positive which means the selected index angle of 18 degree is overall larger than the required blade pitch angle in the covered flight conditions. Therefore, downward deflected flap angles are required to reduce the blade pitch to achieve the prescribed rotor thrust level. As expected, smaller collective flap angles are needed in simulated positive large g-level flights (i.e. g-level of 0.3) where large blade pitch angles are required. Contrarily, larger collective flap angles are required in negative g-level flights. The collective flap angles of high forward speed ( $\mu = 0.16$ ) is overall smaller than that of the low forward speed ( $\mu = 0.08$ ). This is again because smaller collective flap angles are required at high speed which need larger blade pitch angle. Figure 4(b) examines the lateral cyclic flap angles under different g-level of maneuvering flights. Lateral cyclic flap angles shows small increase with g-level at low speed ( $\mu = 0.08$ ). At high speed ( $\mu = 0.16$ ),

lateral cyclic flap shows a higher sensitivity with g-level, however, is still relatively small (less than 2 degrees). Figure 4(c) shows the magnitude of longitudinal cyclic flap angles increase with g-level, and its sensitivity with g-level is again larger with higher speed. This is because of the cyclic blade pitch motion generated by flap collective angle in forward flight conditions. Large downward deflected flap collective shown at negative g-level flight (Fig. 4(a)) produces relatively large blade longitudinal cyclic pitch motion in high speed flights which in turn, require longitudinal flap cyclic deflections to compensate. Figure 4(d) evaluates the actuation power requirements of trailing-edge flap system in simulated maneuvering flights with different g-levels. As expected, large negative g-level flight requires the most actuation power because of the large cyclic flap angles needed, especially at high speed.

Figure 5 examines trailing-edge flap angles and actuation power required at various shaft tilt angles. Different longitudinal shaft tilt angles are prescribed in wind tunnel trim to simulate descending and ascending forward flight conditions. Figure 5(a) presents collective flap angles required for two flight speeds at different shaft tilt angles. Larger collective angle are required at descending flight conditions simulated with backward tilted rotor shaft, especially for high speed. It is noted that high speed ( $\mu = 0.16$ ) in wind tunnel trim essentially simulated higher descending rate than the low speed with same shaft tilt angle. Figure 5(b) shows the lateral cyclic flap angles have larger sensitivity with high speed, however, are overall small in the covered shaft tilt angles. Figure 5(b) evaluates the longitudinal cyclic flap angle at different different shaft tilt angles. Large longitudinal cyclic flap angles are required in simulated descending flight at high speed ( $\mu = 0.16$ ). In low speed ( $\mu = 0.08$ ), it is shown that longitudinal cyclic flap angle presents small variation with shaft tilt angle. Accordingly, Figure 5(d) shows large actuation power is required at descending flight at high speed, and small variation of actuation power is again shown with low speed ( $\mu = 0.08$ ).

Figure 6 examines the effect of pitch index angle on actuation requirements of trailing-edge flap system in maneuvering flights. Results of three g-levels (0, 0.3 and -0.3) are presented. Zero g-level simulates the steady level forward flight condition. Figure 6(a) presents that collective flap angles increase with increasing pitch index angle, and shows the same sensitivity with the pitch index angle for all three g-level cases. Negative g-level maneuvering flight requires overall larger collective flap angle than the zero g-level because of less blade pitch angle required. Similarly, positive g-level flight needs overall smaller than zero g-level because of larger blade pitch angle required in such flight conditions. Figure 6(b) illustrates variation of lateral cyclic flap angles with

pitch index angles. Lateral cyclic flap angles decrease with increasing pitch index angle. Positive g-level flight requires largest lateral cyclic flap angles among the three g-level flight conditions. Figure 6(c) compares variation of longitudinal cyclic flap angles with index angle with simulated three g-level maneuvering flights. The longitudinal cyclic flap angles are closed related with collective flap angle in high speed flights ( $\mu = 0.16$ ). This is again because of the longitudinal cyclic blade pitch motion induced by collective flap angle in forward flights. It is shown that positive g-level flights requires overall largest longitudinal cyclic flap angles among the three different flight conditions. Figure 6(d) shows variation of actuation power of trailing-edge flap system with blade pitch index angles. As expected, minimum of actuation powers of three flight conditions locate in different blade index angle. Positive g-level flights have the largest optimum blade index angle at  $18^\circ$ , and zero g-level and negative g-level flight conditions respectively presents the optimum blade index angle at  $16^\circ$  and  $12^\circ$ . It is shown that the selection of blade index angle is a comprise among flight conditions, i.e. steady-level flights, maneuvering flights, and flight speeds.

## Autorotation Flights

Autorotation flights are simulated with wind tunnel trim by adjusting shaft tilt angle to achieve zero rotor mast torque. Figure 7 examines the actuation requirements of trailing-edge flap system in autorotation flights at different forward speeds. Figure 7(a) compares variation of collective flap angles with forward speed using three main rotor rpm (100%, 110% and 90% of nominal rpm). It is shown collective flap angles slightly increases with forward speed. Slower rotor rpm (90%) has the overall largest collective flap angles with the maximum of  $7.5^\circ$  at  $\mu = 0.16$ . Figure 7(b) shows that the required lateral cyclic flap angles at different forward autorotation flight speeds are again overall small. Figure 7(c) shows that the magnitude of longitudinal cyclic trailing-edge flap angles increase with forward speeds. This is to compensate the longitudinal cyclic blade pitch motion induced by collective trailing-edge flap angle in forward flights. The required longitudinal cyclic flap angles shows the same trend and has close values among the three rotor rpm cases, especially between cases of 100%rpm and 110%rpm. Figure 7(d) presents actuation power of trailing-edge flap system required in autorotation flights at different speeds. Larger actuation power is required at high speeds because of the larger magnitude of longitudinal cyclic flap angle shown in Fig. 7(c). Actuation power of 90%rpm case is overall the largest among the three rotor speeds. It is noted that autorotation is normally performed at low speed in practice which has

relatively small actuation power.

## Conclusions

This paper examines the actuation requirements of trailing-edge flap system as primary flight control device for an ultralight helicopter rotor in maneuvering and autorotation flights. Wind tunnel trim procedure is adopted to simulate these flight conditions. The requirements of trailing-edge flap angles and actuation power are studied in different g-level maneuvering flights and various shaft tilt angles which are used to simulate descending and ascending forward flights. The effects of key design variable, pitch index angle, on trailing-edge flap deflections and actuation power are investigated in maneuvering flights. The following conclusions are subject to the limitations of the analysis and the scope of the study:

1. With the selection of pitch index angle of  $18^\circ$ , moderate trailing-edge flap deflection and actuation power is required at maneuvering flights with small g-levels, especially at low speed.
2. Selection of optimum blade index angle is a comprise among flight conditions, i.e. steady-level and maneuvering flights.
3. With the design of trailing-edge flap system, which consists of an  $18\%R$  plain flap with  $25\%$  chord ratio located at  $82\%R$ , the trailing-edge flap deflections required to trim the rotor in simulated autorotation conditions are moderate in low speed which most autorotation performed in practice. Collective trailing-edge flap angle is of  $5.6^\circ$  and both longitudinal and lateral cyclic flap angles are less than  $1^\circ$  at advance ratio of 0.05 with nominal rotor speed. Accordingly, actuation requirements are also small in this case.

## Acknowledgments

This work was supported by the NASA/Ames under grant NGT252273 with Dr. Chee Tung as technical monitor.

## References

<sup>1</sup>Chopra, I., "Status of Application of Smart Structures Technology to Rotorcraft Systems," *Journal of the American Helicopter Society*, Vol. 45, (4):228–252, October 2000.

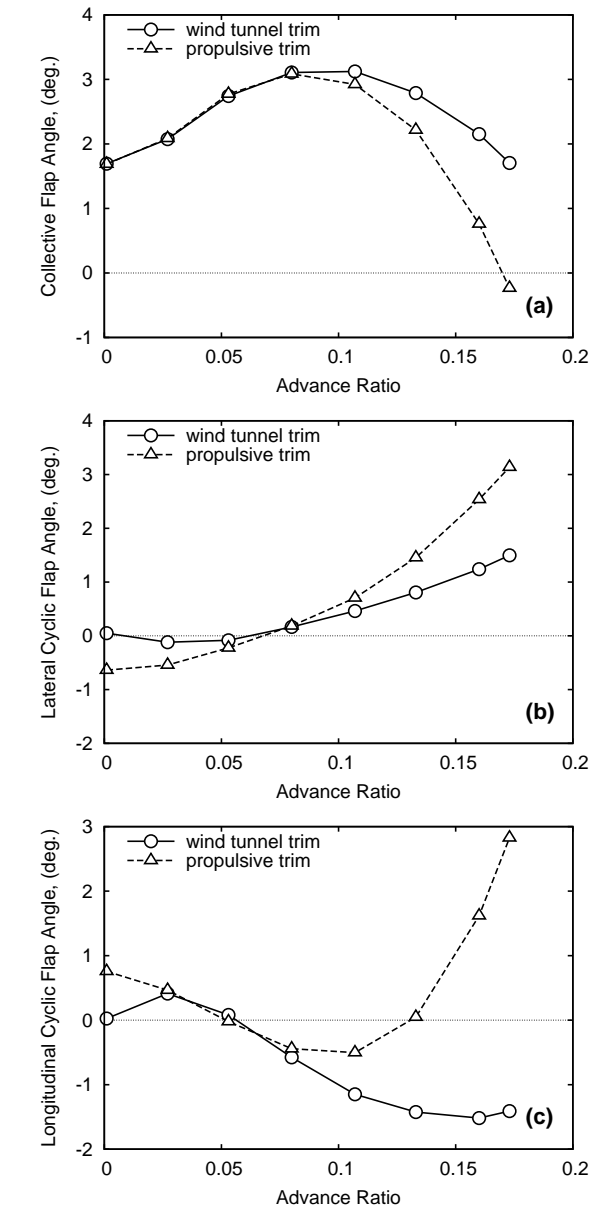


Figure 3: Comparisons of wind tunnel trim and propulsive trim of washplateless rotors for different flight speeds

<sup>2</sup>Straub, F. K. and Charles, B. D., "Aeroelastic Analysis of Rotors with Trailing Edge Flaps Using Comprehensive Codes," *Journal of the American Helicopter Society*, Vol. 46, (3):192–199, July 2001.

<sup>3</sup>Prechtel, E. F. and Hall, S. R., "Design of a High Efficiency, Large Stroke, Electromechanical Actuator," *Smart Materials and Structures Journal*, Vol. 8, (1):13–30, February 1999.

<sup>4</sup>Fulton, M. V. and Ormiston, R. A., "Hover Testing of a Small-Scale Rotor with On-Blade Elevons," *Journal of the*

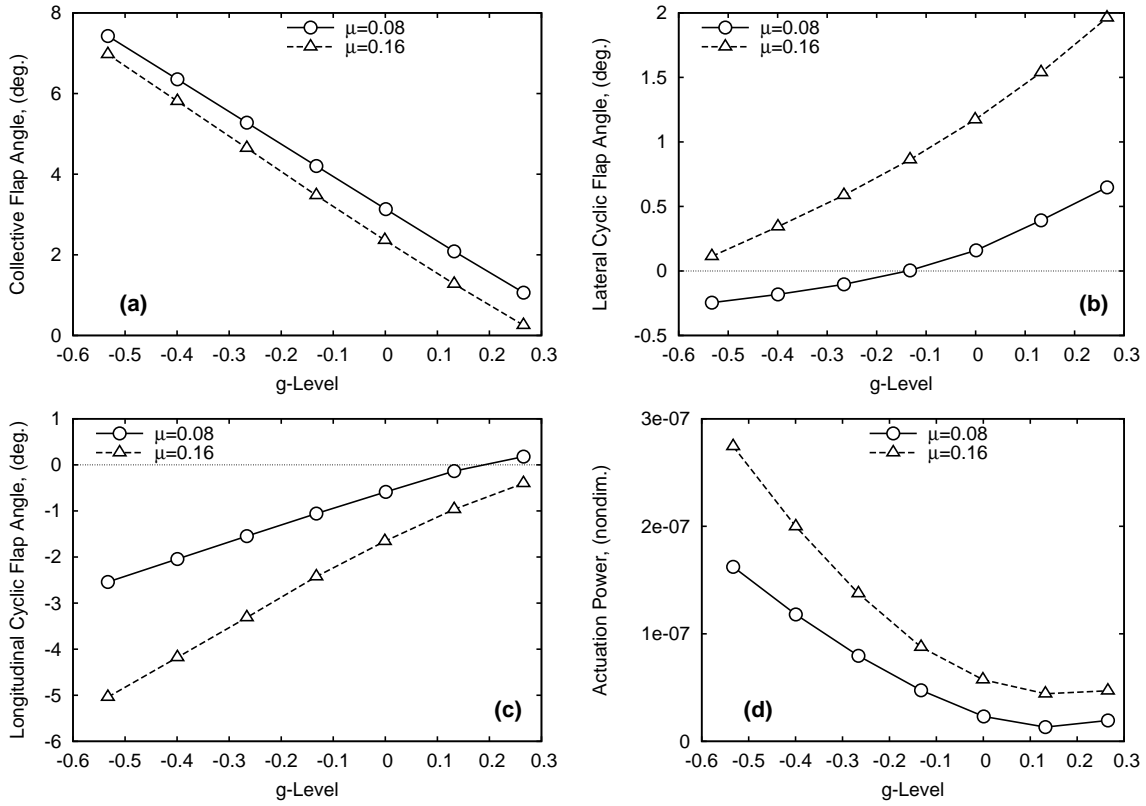


Figure 4: Trailing-edge flap angles and actuation power for different g-levels

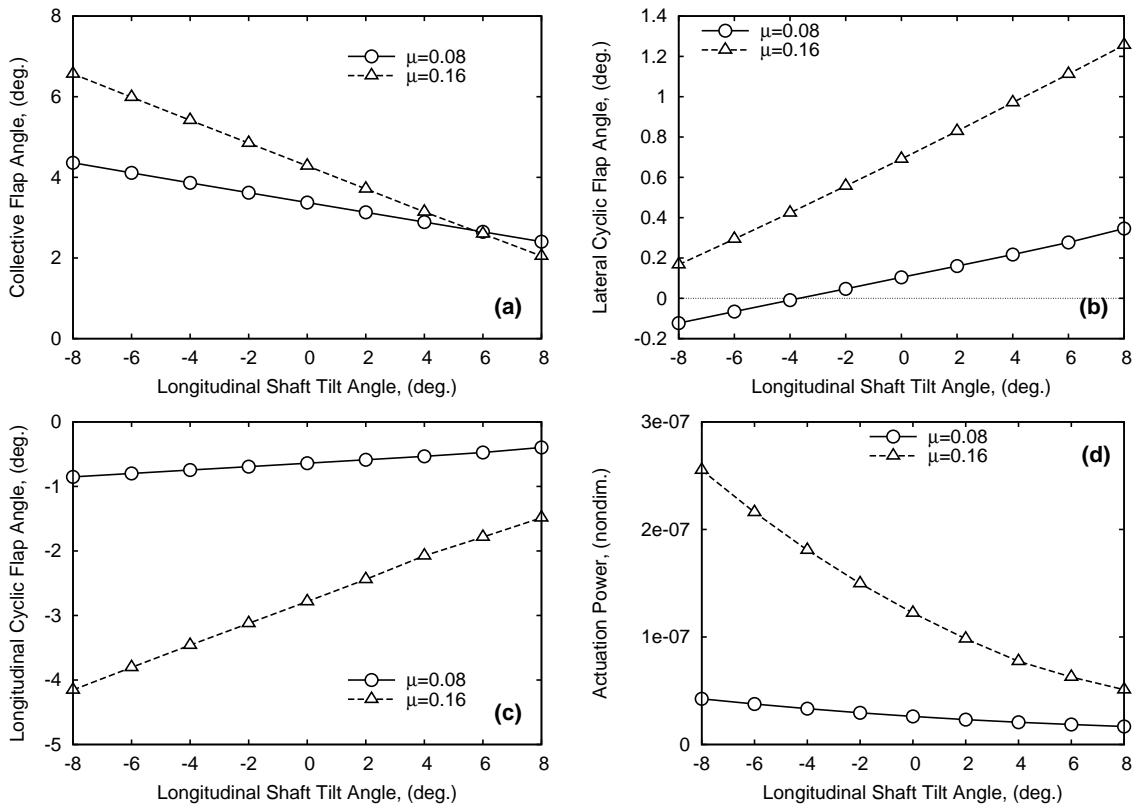


Figure 5: Trailing-edge flap angles and actuation power for different shaft tilt angles

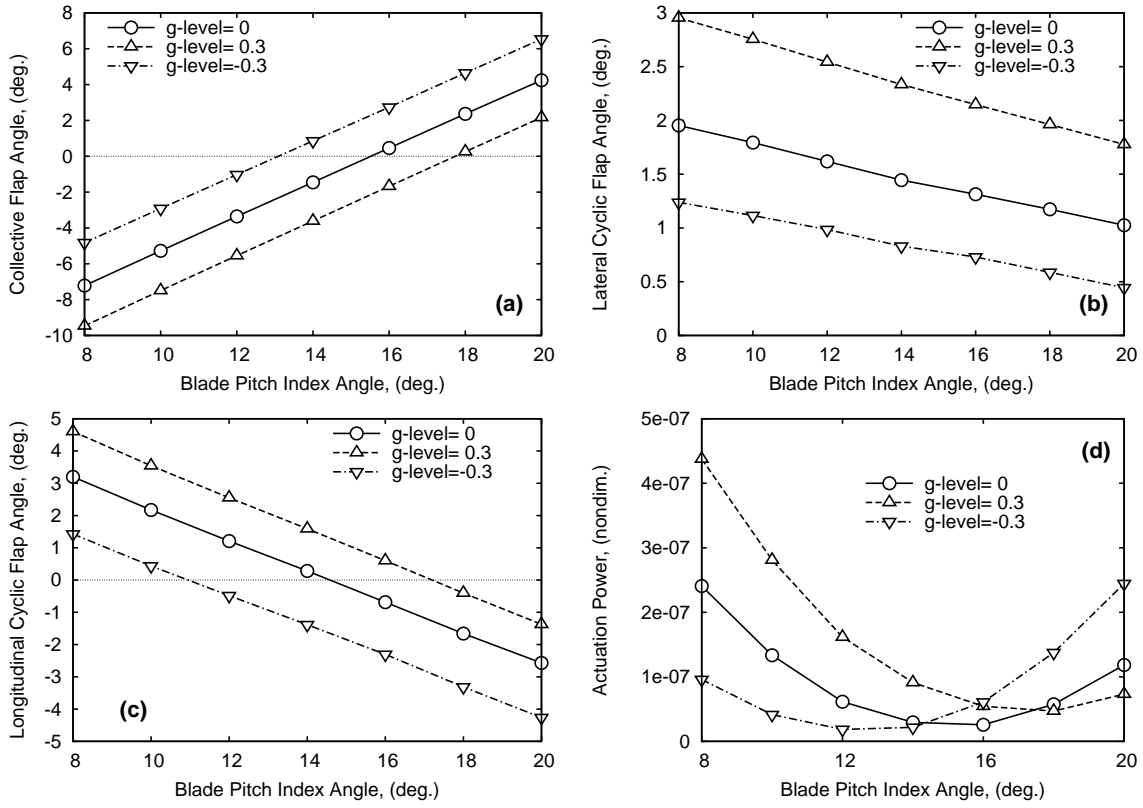


Figure 6: Trailing-edge flap angles and actuation power for different pitch index angles,  $\mu = 0.16$

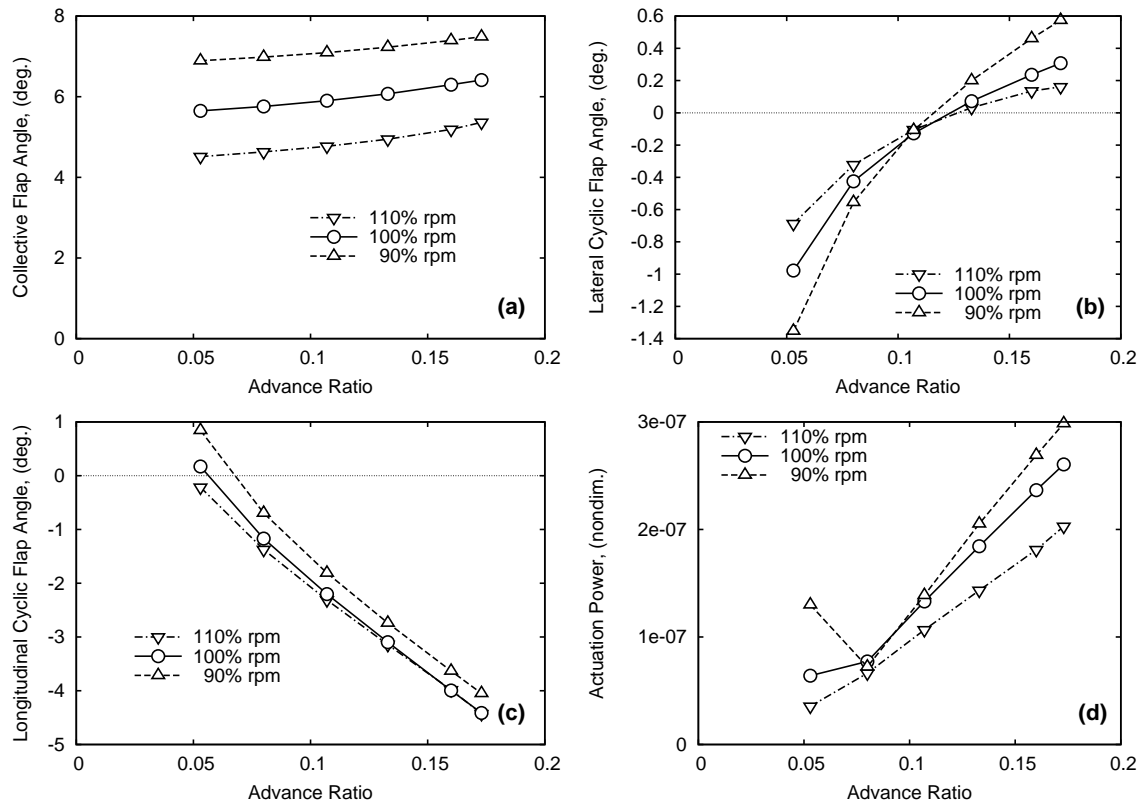


Figure 7: Trailing-edge flap angles and actuation power in autorotation conditions

*American Helicopter Society*, Vol. 46, (2):96–106, April 2001.

<sup>5</sup>Koratkar, N. A. and Chopra, I., “Wind Tunnel Testing of a Mach-Scaled Rotor Model with Trailing-Edge Flaps,” *Journal of the American Helicopter Society*, Vol. 47, (4):263–272, October 2002.

<sup>6</sup>Bernhard, A. and Chopra, I., “Hover Test of a Mach-Scale Rotor Model with Active Blade Tips,” *Journal of the American Helicopter Society*, Vol. 47, (4):273–284, October 2002.

<sup>7</sup>Epps, J. J. and Chopra, I., “In-Flight Tracking of Helicopter Rotor Blades Using Shape Memory Alloy Actuators,” *Smart Materials and Structures Journal*, Vol. 10, (1):104–111, February 2001.

<sup>8</sup>Shen, J. and Chopra, I. “A Parametric Design Study for a Swashplateless Helicopter Rotor with Trailing-Edge Flaps,”. In *American Helicopter Society 58th Annual Forum Proceedings*, page 15, Montreal, Canada, June 11-13 2002.

<sup>9</sup>Barrett, R., Schliesman, M., and Frye, P. “Design, Development and Testing of a Mini Solid State Adaptive Rotorcraft,”. In *SPIE Symposium on Smart Structures and Materials, Conference on Smart Structures and Integrated Systems*, pages 231–242, San Diego, CA, March 1997.

<sup>10</sup>Ormiston, R. A. “Aeroelastic Considerations for Rotorcraft Primary Control with On-Blade Elevons,”. In *American Helicopter Society 57th Annual Forum Proceedings*, Washington, D.C., May 9-11 2001.

<sup>11</sup>Shen, J. and Chopra, I. “Actuation Requirements for a Swashplateless Helicopter Control System With Trailing-Edge Flaps,”. In *Proceeding of the 43rd AIAA/ASME/ASCE/AHS structures, structural dynamics, and materials conference and 10th AIAA/ASME/AHS adaptive structures conference*, number AIAA-2002-1444, page 11, Denver, Colorado, April 2002.

<sup>12</sup>Shen, J. and Chopra, I. “Ultralight Helicopter with Trailing-Edge Flap for Primary Control,”. In *Proceedings of American Helicopter Society International Meeting on Advanced Rotorcraft Technology and Life Saving Activities*, page 10, Tochigi, Japan, November 2002.

<sup>13</sup>Shen, J., Chopra, I., and Johnson, W. “Performance of Swashplateless Ultralight Helicopter Rotor with Trailing-edge Flaps for Primary Flight Control,”. In *American Helicopter Society 59th Annual Forum Proceedings*, page 11, Phoenix, AZ, May 6-8 2003.

<sup>14</sup>Houston, S. S., “Modeling and Analysis of Helicopter Flight Mechanics in Autorotation,” *Journal of Aircraft*, Vol. 40, (4):675–682, July-August 2003.

<sup>15</sup>Yeo, H. and Chopra, I., “Coupled Rotor/Fuselage Vibration Analysis for Teetering Rotor and Test Data Comparison,” *Journal of Aircraft*, Vol. 38, (1):111–121, Jan-Feb 2001.

<sup>16</sup>Hariharan, N. and Leishman, J. G. “Unsteady Aerodynamics of a Flapped Airfoil in Subsonic Flow by Indicical Concepts,”. In *Proceedings of the 36<sup>th</sup> AIAA/ASME/ASCE/AHS/ASC structure, structural dynamics, and materials conference*, New Orleans, LA, April 1995.

<sup>17</sup>Theodorsen, T. and Garrick, I. E. “Nonstationary Flow about a Wing-Aileron-Tab Combination Including Aerodynamic Balance,” Technical Report No. 736, NACA, 1942.

<sup>18</sup>Hassan, A. A., Straub, F. K., and Noonan, K. W. “Experimental/Numerical Evaluation of Integral Trailing Edge Flaps for Helicopter Rotor Applications,”. In *American Helicopter Society 56th Annual Forum Proceedings*, pages 84–102, Virginia Beach, VA, May 2-4 2000.